CISAS "G.COLOMBO"
Centro Interdipartimentale Studi e Attività Spaziali
Università degli Studi di Padova

*Asymptotic analysis of the Whistler waves propagation in space plasma thrusters**

A Cardinali[1], D. Melazzi[2], M. Manente[2,3], D. Pavarin[2,3]

[1] Associazione Euratom-ENEA sulla Fusione, Frascati, Rome, Italy

[2] CISAS "G. Colombo" Centro Interdipartimentale Studi e Attività Spaziali, University of Padova, Italy

[3] hit09 S.r.l. Padova, Italy

* *To be published on Plasma Sources Science and Technology, 2013*

Outline

- **1) Plasma Thruster**
  - *HPH.com project (www.hphcom.eu/index.shtml)*
  - *Helicon Plasma Source concept*
- **3) Mathematical model**
  - *Maxwell-Vlasov system of equations*
  - *Cold plasma approximation*
  - *Collisional Damping*
- **4) Asymptotic analysis of the equation system and solution**
  - *Lowest order phase reconstruction*
  - *First order amplitude or wave energy deposition*
- **5) Numerical results and discussion**
- **6) Conclusions**

Helicon Plasma Hydrazine.combined-micro (HPH.COM) 1/2

- The aim of the HPH.com project is *to develop a space plasma thrusters based on helicon plasma sources*.
- The great innovation of this technology lies on its extreme scalability, that allows it to be used
  - For small pushes in the position control and satellite-formations attitude,
  - for the primary propulsion for interplanetary probes.
- The uniqueness of the project lies in developing an engine that can operate in high-efficiency / low-thrust with only plasma and plasma-hydrazine in the way of low-efficiency / high-thrust.

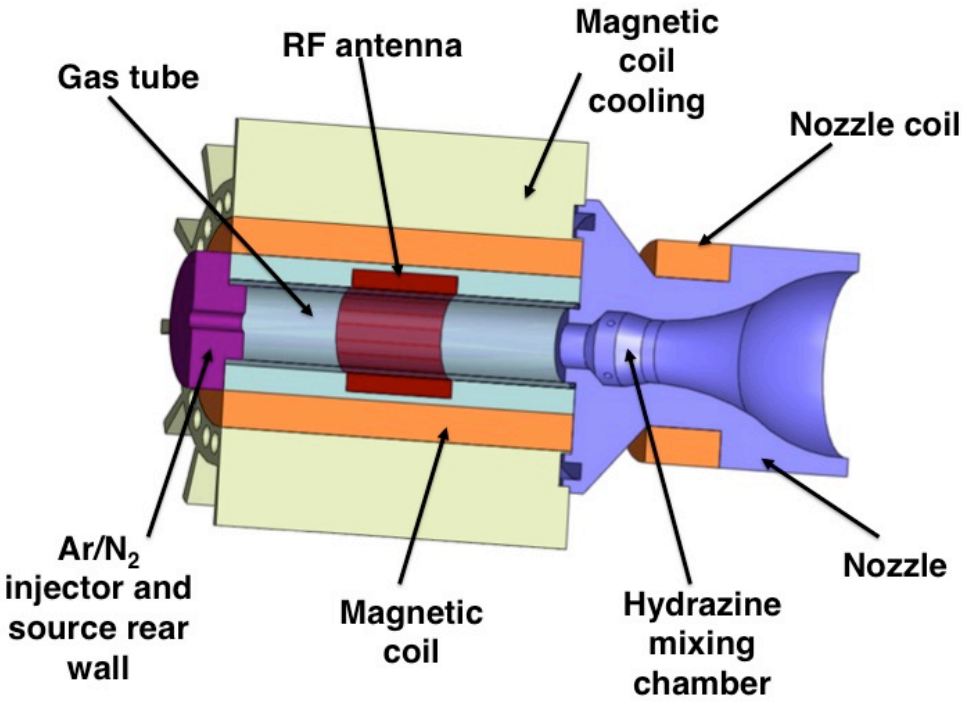

Target Performances		
	Mode I Plasma	**Mode II Plasma + 2nd Prop**
Power(W)	**50 W**	**50**
Thrust (mN)	**1.5 mN**	**20 mN**
Isp (s)	**>1200**	**>400**

Helicon Plasma Hydrazine.combined-micro (HPH.COM) 2/2

- Objective of this research program is to significantly improve knowledge *on helicon-based plasma thruster*
  - through deep numerical/theoretical investigation,
  - through an extensive experimental campaign,
  - through the utilization on board a mini-satellite for attitude and position control.

Helicon Plasma thruster (1/3)

- A Helicon Plasma Thruster or **plasma propulsion engine** is a type of thruster which uses plasma in the thrust generation process.

- A Helicon Plasma Thruster is comprised of
  - (1) Ar/N_2 gas feeding system,
  - (2) RF antenna,
  - (3) magnetic coils

- The RF antenna ionize the neutral gas and heat the resulting plasma via plasma-wave electromagnetic interaction processes.

- Magnetic coils generate divergent magnetic field lines at the exhaust providing a magnetic nozzle effect to focus and accelerate the plasma away from the rocket engine.

Helicon Plasma thruster (2/3)

THE MAGNETIC NOZZLE: Simply stated, a magnetic nozzle converts thermal energy of a plasma into directed kinetic energy. This conversion is achieved using a magnetic field contoured similarly to the solid walls of a conventional nozzle.

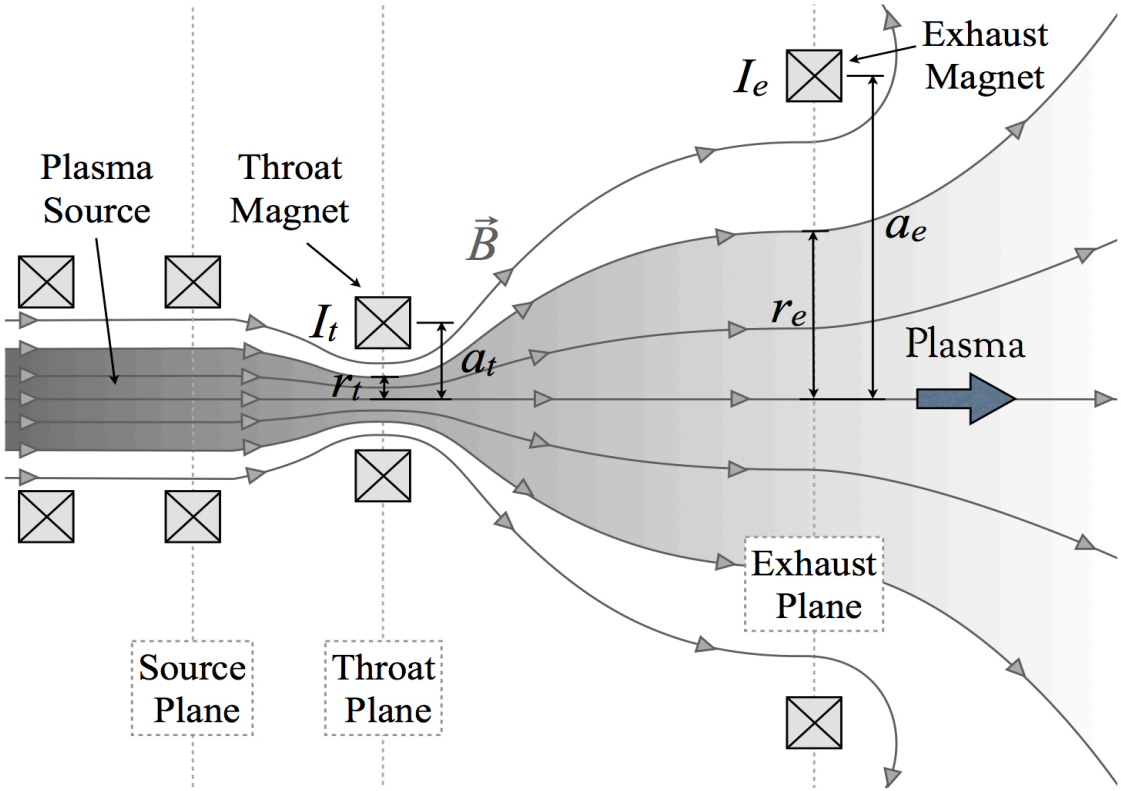

Figure 1. Magnetic Nozzle Schematic

Helicon Plasma thruster (3/3)

THE SOURCE: the plasma source is a Helicon plasma where the confinement magneto-static field is directed **ALONG THE AXIS and in principle is UNIFORM AND CONSTANT (THIS IS NOT TRUE** in actual plasma thruster configuration making the problem of the electromagnetic-plasma interaction to be intrinsically 3D**). The RF antennas excite a Whistler waves at a frequency of 13.56 MHz (HPH.com). The electric field polarization is** E_θ/E_r and the dispersion relation is

$$k_{\parallel}^2 \approx \frac{\omega^2}{c^2}\left(1-\frac{\omega_{pe}^2}{(\omega-|\Omega_{ce}|)(\omega+\Omega_{ci})}\right)$$

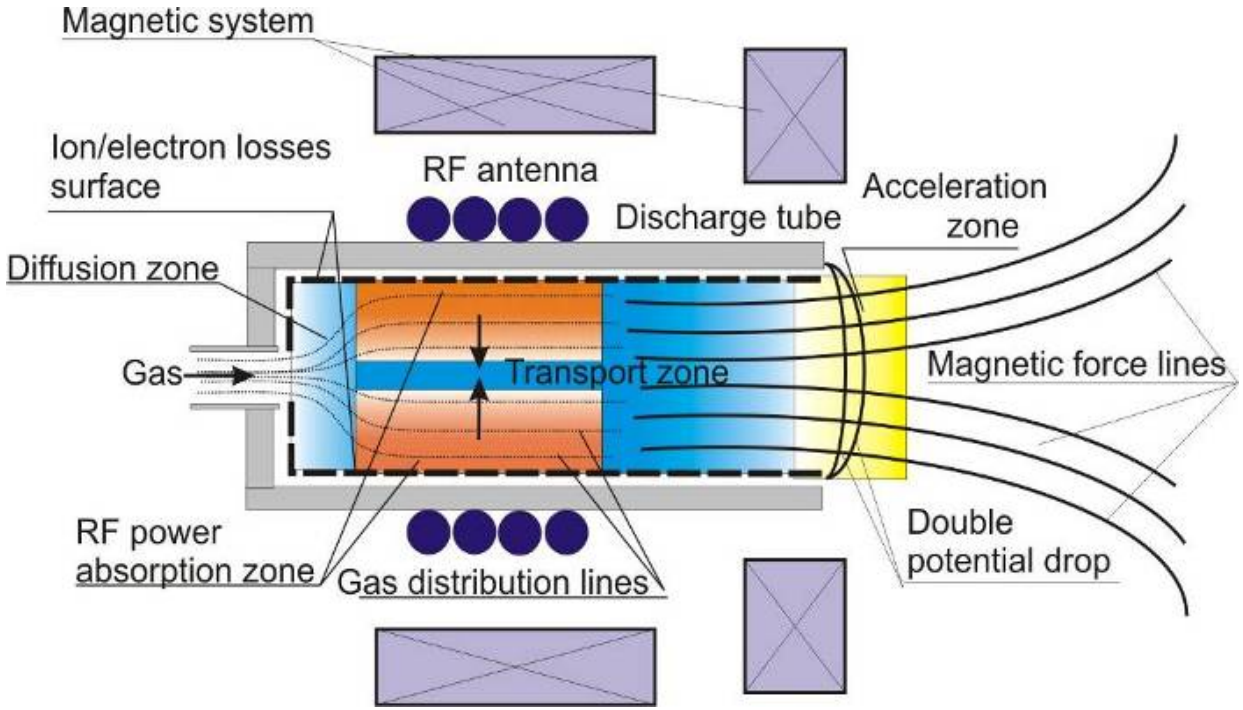

Mathematical model of the plasma-electromagnetic wave interaction in the thruster in presence of an external magnetic field structure

- The equation system which describes the coupling, propagation and absorption of the whistler wave in a cold collisional plasma in presence of an external static magnetic field is the following integro-differential system of equations for the electric field

$$\nabla \wedge \nabla \wedge \vec{E}(\vec{r},t) = -\frac{1}{c^2}\left(\frac{\partial^2 \vec{E}(\vec{r},t)}{\partial t^2} + 4\pi \sum_{\alpha=e,i} q_\alpha n_{0\alpha} \frac{\partial \vec{v}_\alpha}{\partial t} \right)$$

$$\frac{\partial \vec{v}_\alpha}{\partial t} = \Omega_{c\alpha} \vec{v}_\alpha \wedge \vec{b} + \frac{q_\alpha}{m_\alpha} \vec{E} - \nu_{\alpha,\alpha}^{coll} \vec{v}_\alpha$$

- The hypothesis made in obtaining this system to start from the Maxwell-Vlasov equation are:
  - Cold plasma
  - Linearization of the fluid model
  - Inclusion of very simple collisional model (Krook)

Mathematical model 1

- Considering that both electron-ion density and external magnetic field does not depend on time (steady state condition), the system above simplifies considerably.

- **The perturbation quantities can be considered harmonic in time ~$e^{-i\omega t}$**

- The equation system lost the integro-differential character, and becomes a vector partial differential equation of the second order for the electric field components

$$\nabla \wedge \nabla \wedge \vec{E}(\vec{r},t) = \frac{\omega^2}{c^2}\vec{E}(\vec{r},t) + \frac{i\omega}{c^2}\sum_{\alpha=e,i}\omega_{p\alpha}^2 \underline{\underline{M_\alpha}}(\omega,\vec{r})\cdot\vec{E}(\vec{r},t)$$

- Where $\underline{\underline{M_\alpha}}(\omega,\vec{r})$ is the mobility tensor and it depends on the frequency and locally on space!

Mathematical model 2

$$\underline{\underline{M_\alpha}} = \frac{1}{-i\omega^*\left(\omega^{*2}-\Omega_{c\alpha}^2\right)}\begin{bmatrix} \left(i\omega^*\right)^2+\Omega_{c\alpha}^2\left(\hat{b}_1\right)^2 & -\left(i\omega^*\Omega_{c\alpha}\hat{b}_3\right)+\Omega_{c\alpha}^2\left(\hat{b}_1\hat{b}_2\right) & \left(i\omega^*\Omega_{c\alpha}\hat{b}_2\right)+\Omega_{c\alpha}^2\left(\hat{b}_1\hat{b}_3\right) \\ \left(i\omega^*\Omega_{c\alpha}\hat{b}_3\right)+\Omega_{c\alpha}^2\left(\hat{b}_1\hat{b}_2\right) & \left(i\omega^*\right)^2+\Omega_{c\alpha}^2\left(\hat{b}_2\right)^2 & -\left(i\omega^*\Omega_{c\alpha}\hat{b}_1\right)+\Omega_{c\alpha}^2\left(\hat{b}_2\hat{b}_3\right) \\ -\left(i\omega^*\Omega_{c\alpha}\hat{b}_2\right)+\Omega_{c\alpha}^2\left(\hat{b}_1\hat{b}_3\right) & \left(i\omega^*\Omega_{c\alpha}\hat{b}_1\right)+\Omega_{c\alpha}^2\left(\hat{b}_2\hat{b}_3\right) & \left(i\omega^*\right)^2+\Omega_{c\alpha}^2\left(\hat{b}_3\right)^2 \end{bmatrix}$$

where $\omega^* = \omega + i\nu_{\alpha,\alpha}$

Mathematical model and solution 3

- To solve the ***vector partial differential equations*** with given boundary conditions (fixed by the antenna current distribution) is a cumbersome task owing to the 3D geometry (cylinder + nozzle).
- **The main plasma parameters are**
  - Plasma frequency which in turns depends on the plasma density which depends on 2D space $n(r,z)$
  - Cyclotron frequency which depends on the external magneto-static field, which in turns depends on 3D space $B(r,\theta,z)$
- **And they are depending on 3D space coordinate, at least on 2D.**

Mathematical model and solution 4

- Analytical and numerical solution can be given only in very simple situation in which the density depends only on the radial coordinate and the external magnetic field is uniform inside the cylinder chamber.

- In more complex situation both numerical and analytical approaches cannot be carried out. We propose, an analytical treatment of the wave equation which is based on the asymptotic expansion (WKB Ansatz)

$$h << 1 \qquad E(\vec{r}) \approx \left(e^{h^{-1}\sum_{n=0}^{N} h^n S_n(\vec{r})} \right)$$

Mathematical model and solution 5

- If we use the above representation for the field and we insert it in the wave equation, we got a series **of *first order partial differential equation*** for the function S_n.
- The first two functions S_0 and S_1 have an immediate physical meaning:
  - *S_0 is the wave phase surface function*
  - *$exp(iS_1)$ is the wave amplitude*

- Obviously it is necessary to check that the following condition remains verified

$$\left(\left|\frac{1}{S_1}\frac{dS_1}{d\vec{r}}\right|\right)^{-1} >> \left(\left|\frac{1}{S_0}\frac{dS_0}{d\vec{r}}\right|\right)^{-1} \Rightarrow L >> \lambda$$

- Essentially this means that the wavelength of the propagating wave is much smaller then the typical scale length of the amplitude variation.

Mathematical model and solution 6

- After substituting the WKB ansatz in the wave equation, a non-linear partial differential equation for the function S_0 at the lowest order results. The solution can be obtained by the method of characteristics (ray-tracing)

$$\frac{dx}{d\tau} = \delta_0^{-1} \frac{\partial \mathcal{H}}{\partial n_x} \qquad \frac{dn_x}{d\tau} = -\delta_0^{-1} \frac{\partial \mathcal{H}}{\partial x}$$

$$\frac{d\theta}{d\tau} = \frac{\partial \mathcal{H}}{\partial m} \qquad \frac{dm}{d\tau} = -\frac{\partial \mathcal{H}}{\partial \theta}$$

$$\frac{d\hat{z}}{d\tau} = \delta_0^{-1} \frac{\partial \mathcal{H}}{\partial n_z} \qquad \frac{dn_z}{d\tau} = -\delta_0^{-1} \frac{\partial \mathcal{H}}{\partial \hat{z}}$$

$$\frac{dt}{d\tau} = \frac{\partial \mathcal{H}}{\partial \omega} \qquad \frac{d\omega}{d\tau} = -\frac{\partial \mathcal{H}}{\partial t} = 0 \Rightarrow \omega = const$$

$$\frac{d\mathcal{S}_o}{d\tau} = n_x \frac{\partial \mathcal{H}}{\partial n_x} + m \frac{\partial \mathcal{H}}{\partial m} + n_z \frac{\partial \mathcal{H}}{\partial n_z}$$

Mathematical model and solution 7

- Incidentally, the ray tracing equations (which are a system of ordinary differential equations of the first order) are formally equivalent to the Hamilton's equation of the classical mechanics, and the non linear partial differential equation for the function S_0 is equivalent to the Hamilton-Jacobi equation. The Hamiltonian results to be

$$\mathcal{H} \equiv A\left(\vec{r}, \left|\nabla_{\parallel} S_0\right|\right)\left|\nabla_{\perp} S_0\right|^4 + B\left(\vec{r}, \left|\nabla_{\parallel} S_0\right|\right)\left|\nabla_{\perp} S_0\right|^2 + C\left(\vec{r}, \left|\nabla_{\parallel} S_0\right|\right) = 0$$

- ***The wave dispersion relation***

Mathematical model and solution 8

- At the successive order in h we obtain a partial differential equation of the first order for S_1. This amplitude transport equation can be recast in an equation for the wave power transported along the trajectory, which satisfies the "Poynting theorem".

$$\frac{dP}{dt} = -2\gamma_{new}\left(\boldsymbol{r},\boldsymbol{k},\omega\right)P\,, \qquad P = \frac{\omega}{16\pi}\int d\boldsymbol{\Sigma}\cdot\frac{\partial\mathcal{H}\left(\boldsymbol{k},\omega\right)}{\partial\boldsymbol{k}}\left|\boldsymbol{\mathcal{A}}_0\right|^2$$

$$\gamma_{new}\left(\boldsymbol{r},\boldsymbol{k},\omega\right) = \frac{\boldsymbol{e}_0^*\cdot\varepsilon^A\left(\boldsymbol{r}\right)\cdot\boldsymbol{e}_0}{\partial\mathcal{H}\left(\boldsymbol{k},\omega\right)/\partial\omega}$$

Numerical solution of the WKB ordinary differential equations: application to HPH.com plasma thruster

- **We considered three different configurations for the wave propagation and power deposition analysis:**
  - (a) 2D confinement magnetic field and 1D radial density profile,
  - (b) 2D confinement magnetic field and 2D density profile,
  - (c) axial, uniform and constant confinement magnetic field and 1D radial density profile (helicon case).

- **These configurations have been reported in Tab. 1. Each test label is used as label for the curves in the following pictures.**

Label	Density profile	Confinement magnetic field
a)	radial	$B_r(r,z)\,\boldsymbol{e_r} + B_z(r,z)\,\boldsymbol{e_z}$
b)	radial & axial	$B_r(r,z)\,\boldsymbol{e_r} + B_z(r,z)\,\boldsymbol{e_z}$
c)	radial	$B_0\boldsymbol{e_z} = \text{const}$

Numerical solution of the WKB ordinary differential equations, and results: wavenumber evolution

The axial wavenumber n_z evolution:

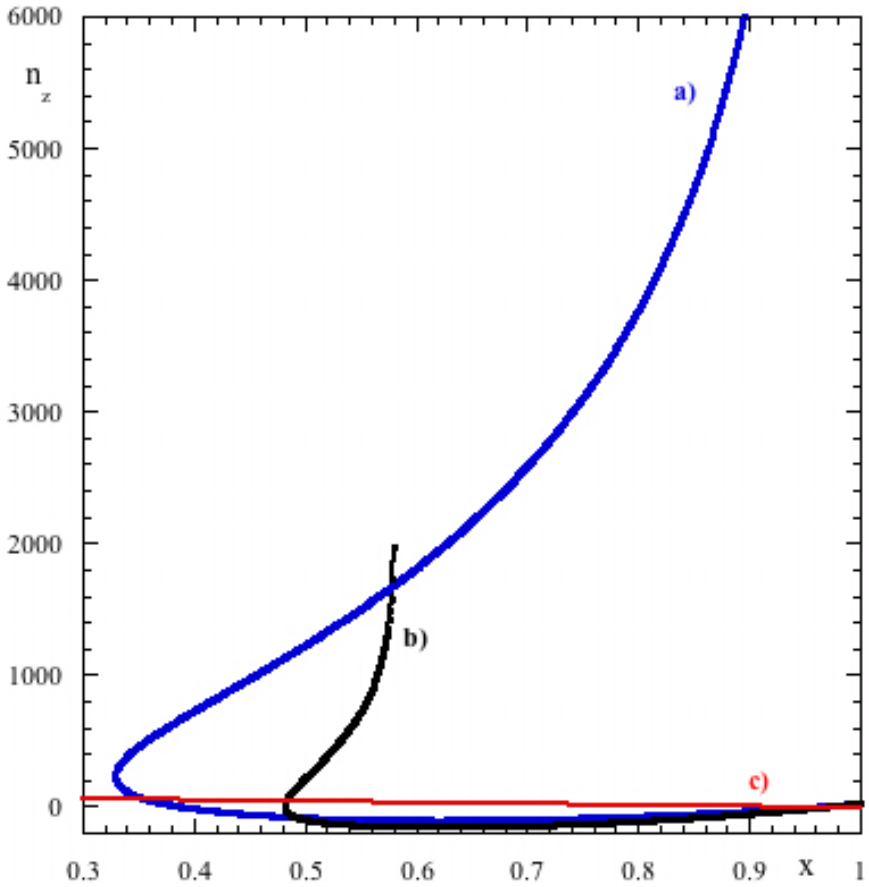

In the **c) case (red line)**, the axial wavenumber remained constant inside the plasma. In **a) (blue line)** and **b) (black line)** the magnetic field induces a variation of the axial wavenumber along the ray.

In the **case a)**, after a radial reflection, an axial resonance appears near the plasma edge, while in the **case b)** the resonance appears just after the radial reflection.

Numerical solution of the WKB ordinary differential equations, and results: wavenumber evolution

the parallel wavenumber $n_{||}$

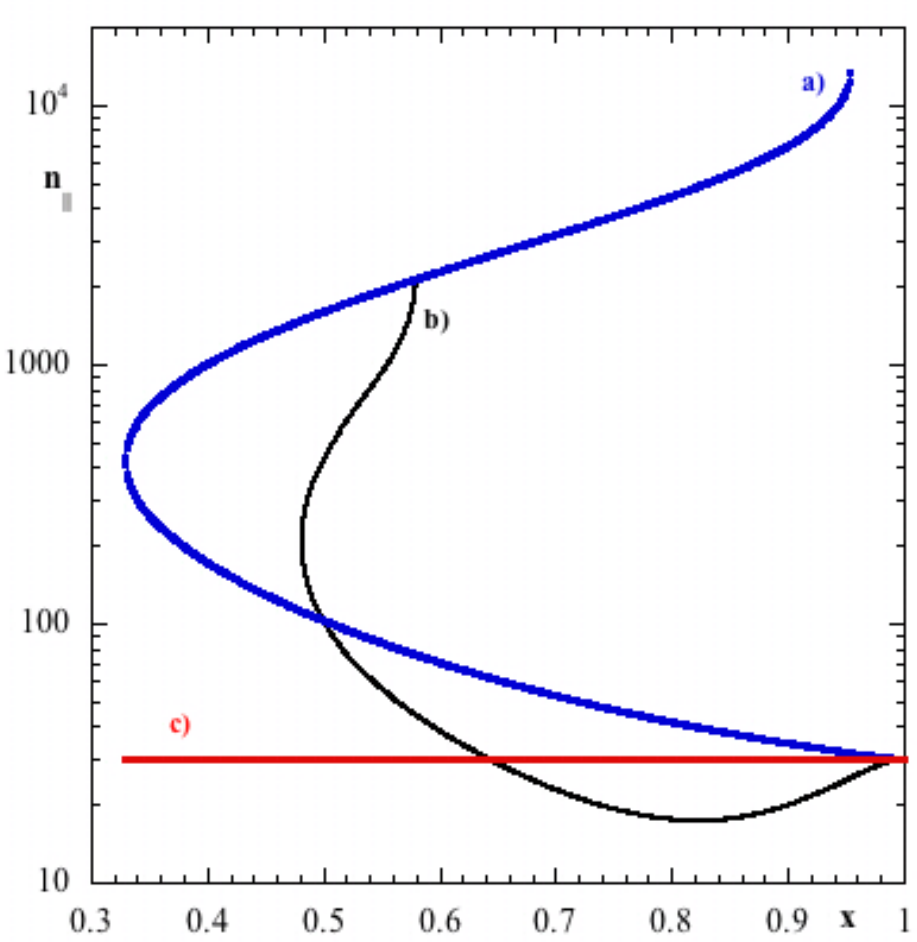

The parallel wavenumber shows the same behavior:

c) case (red line), the parallel wavenumber remained constant inside the plasma.

a) (blue line) and **b) (black line)** the magnetic field induces a variation of the parallel wavenumber along the ray.

In the **case a) and b)** a resonance is met in parallel direction

Numerical solution of the WKB ordinary differential equations, and results: wavenumber evolution

the perpendicular wavenumber $n_\perp$

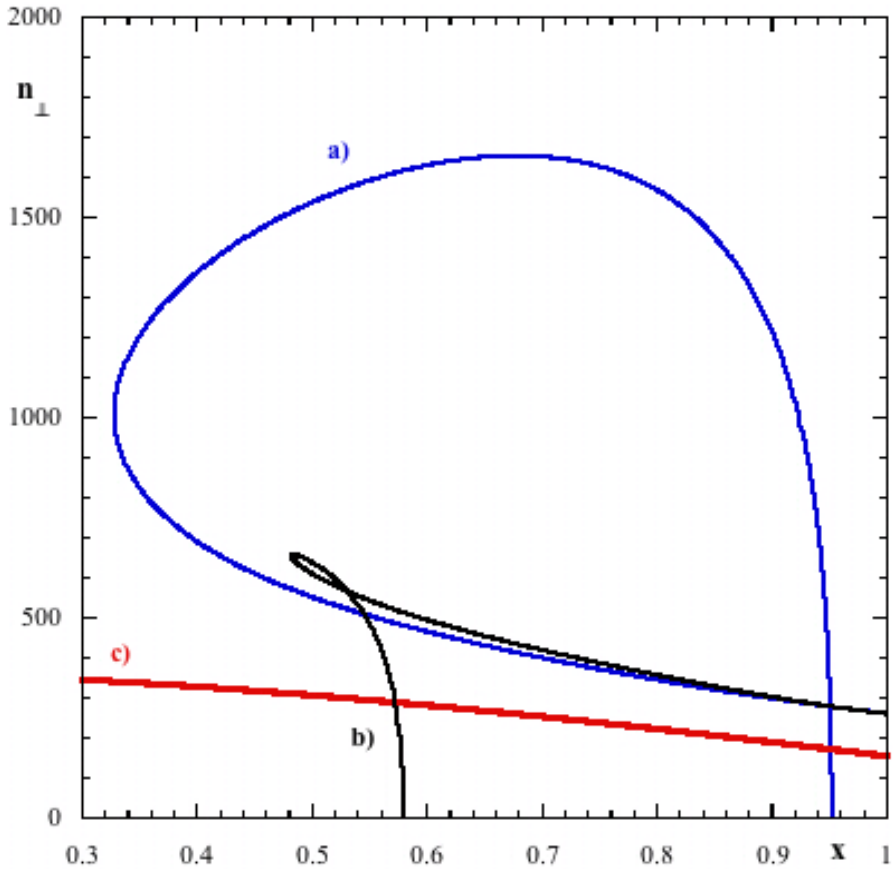

In the **c) case (red line)**, the perpendicular wavenumber varies weakly along the plasma radius.

In **a) (blue line)** and **b) (black line)** the magnetic field structure induces a strong variation of the perpendicular wavenumber during the wave propagation.

In the **case a),** after a radial reflection, a cut-off appears near the plasma edge, while in the **case b)** the cut-off appears just after the radial reflection.

Numerical solution of the WKB ordinary differential equations, and results: power damping rate and power deposition profiles

- ***We discuss the wave absorption features related to cases a).***

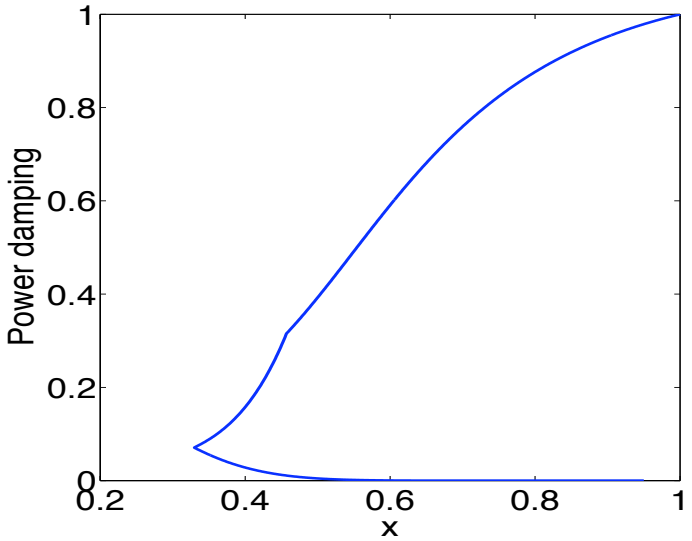

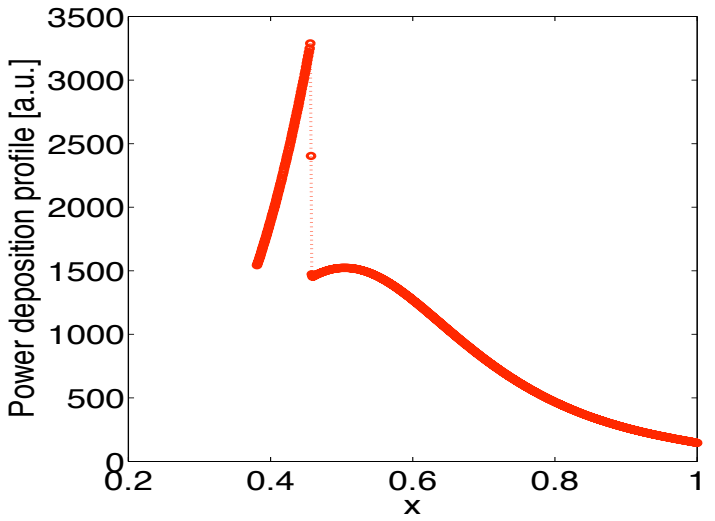

- In this figure the power damping is pictured for a ray path such that the wave gets reflected radially and gets back to x≈1 (edge). Two particular points can be identified.
  - The first one is around x≈0.3 where the wave is reflected radially.
  - The second point is at x ≈ 0.5 where the ***fast wave couples to a slow wave***.
- At the second point, the power damping curve changes its slope, and this is related to the different ways the slow and the fast wave modes deposit energy into the plasma.

- *This feature becomes even more evident in the figure below, where the power deposition profile is pictured for the same case of the above figure.*

Numerical solution of the WKB ordinary differential equations, and results: power damping rate and power deposition profiles

- *We discuss the wave absorption features related to cases b).*

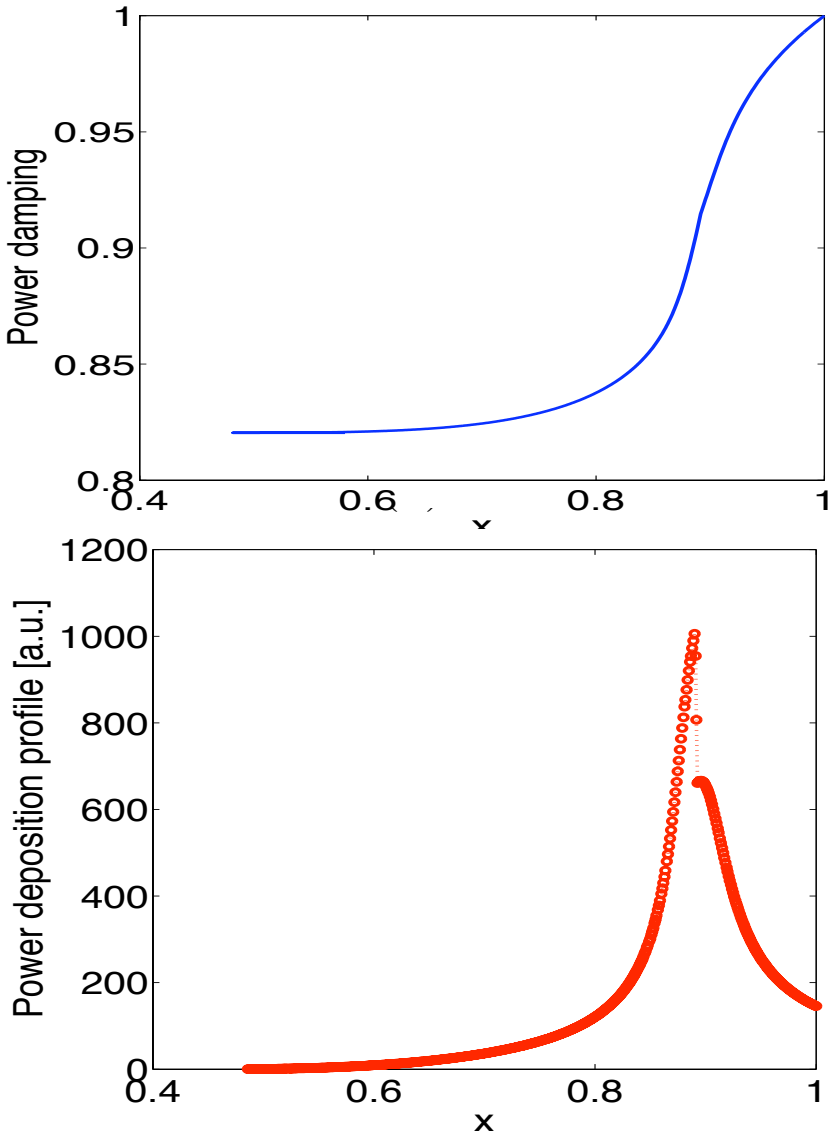

- In this figure the power damping has been pictured for a ray path such that the wave gets reflected radially and gets back up to x ≈ 0.6.
- From the figure just one particular point can be identified, which is at x ≈ 0.5, where the wave is reflected radially.
- There is actually another point at x ≈ 0.9, where the fast wave launched at the edge couples to a slow wave.
- This feature is not easily visible on the figure, where there is no clear change in the slope of the power damping curve; however, it can be clearly recognized in the jump in the power deposition profile showed in the figure below.
- After the mode conversion, the slow wave is rapidly damped by collisions before reaching the axis.

Conclusions

- We developed a three-dimensional Ray-Tracing solver called RAYWh, and we used it to study - for the first time - the whistler propagation and power deposition in a cylindrically-shaped plasma source for space plasma thrusters, where realistic density profiles and confinement magnetic field lines can be readily included without any approximation.

- Previous approaches cannot provide accurate information on the power deposited into the plasma, when real thruster setups are considered. Indeed, magnetic confinement configurations in actual HPTs can depart from the simplified Helicon one, due to dimension, mass and power budget limitations, leading to different power coupling levels into the plasma, and resulting in different propulsive characteristics.

- **Unlike the helicon case, parallel and perpendicular wavenumbers changed during the wave trajectory leading to a completely different propagative picture, when actual confinement magnetic configurations and plasma density profiles are considered.**
  - Unexpected cut-offs, resonances, radial reflections, and mode conversions of the excited waves have been found, as a result of the confinement magnetic field along with variation in the plasma density the waves encountered.
  - These in turn influenced the power deposition phenomena. The results are relevant for space thruster applications, but they can be fruitfully employed in industry plasma sources as well for the identification of the best source configuration, thus providing the maximum power transfer from the RF antenna to the plasma.